

Supplemental materials for "Quantum anomalous Hall effect and tunable topological states in 3d transition metals doped silicene"

Xiao-Long Zhang, Lan-Feng Liu, and Wu-Ming Liu
 Beijing National Laboratory for Condensed Matter Physics,
 Institute of Physics, Chinese Academy of Sciences, Beijing 100190, China
 (Dated: October 31, 2018)

COMPUTATIONAL METHOD

The first-principles calculations are performed based on the density functional theory (DFT) [1] with generalized gradient approximation (GGA) in the form of Perdew-Burke-Ernzerhof (PBE) functional [2] as implemented in Vienna Ab-initio Simulation Package (VASP) [3]. The GGA + U method which treats the on-site repulsion interactions of 3d electrons in a mean field manner is used to evaluate the strong correlation effect in TM, and a typical value of $U = 4$ eV and $J = 0.9$ eV are used for all TM concerned [4]. The lattice constant $a = 3.86$ Å of silicene and the buckling distance $\delta = 0.44$ Å are obtained corresponding to the global minima on the Born-Oppenheimer surface, which agree with existing theoretical data [5, 6]. As to the structure relaxation, all atoms are allowed to relax freely along all directions and all parameters are chosen to converge the forces to less than 0.01 eV/Å. A vacuum space of 20 Å is set to prevent the interaction between silicene and its periodic images along c -axis. Convergence tests with respect to energy cutoff and k points sampling are performed to ensure numerical accuracy of total energy. We find an energy cutoff of 420 eV and Γ centered Monkhorst-Pack grids of $8 \times 8 \times 1$ for k point sampling are enough to converge the difference in total energy to around 1 meV.

IMPACT OF STRONG CORRELATION EFFECT ON ADSORPTION STRUCTURE AND MAGNETIC MOMENTS

For the sake of comparison, we define bond lengths (d_{Si-TM}) as the distance between adatom and the 3 nearest neighbour Si atoms to it, adsorption height (h_{Si-TM}) as the distance between adatom and the lower sublattice (averaged) in c -axis for all 3 adsorption sites, height above Si atom (δ_{Si-TM}) as the distance between adatom and the Si atom underneath for T_A and T_B sites (Fig. 1).

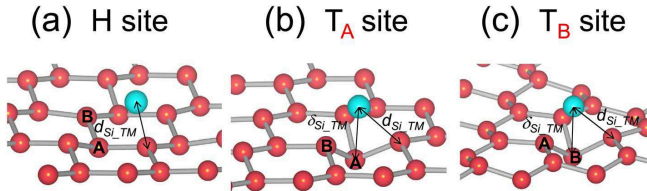


FIG. 1. Schematic representation of bond parameters (d_{Si-TM} and δ_{Si-TM}) for 3 adsorption sites (a) H, (b) T_A , and (c) T_B , respectively.

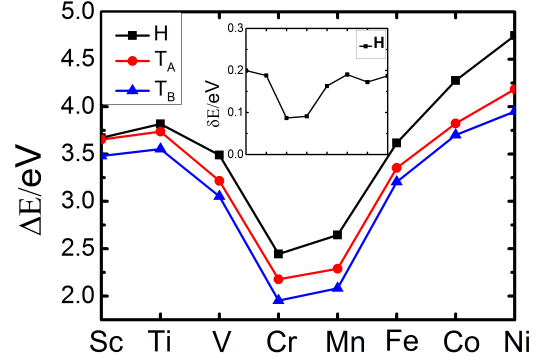


FIG. 2. The adsorption energy (ΔE) of all 3d transition metals (TM) adsorbed on the three high symmetric sites of silicene monolayer, H, T_A and T_B , in the GGA level. The inset shows the distortion energy (δE) of silicene when different TM are situated on the stable site H.

In the GGA case, as can be seen from Fig. 3(a), the bond lengths and adsorption height generally decrease with increasing of atomic number when TM adsorbing on H site. However, the adsorption energy doesn't follow this trend (Fig. 2), which has minimal value of 2.44 eV for Cr and maximal value of 4.75 eV for Ni. We can see from inset in Fig. 2 that the above trend of adsorption energy is correlated to the different distortion of silicene, which is energetically characterized by the distortion energy defined as $\delta E = E_{dis} - E_s$, where E_{dis} is the energy of silicene after adsorption. The distortion energy are small for V and Cr, suggesting relatively weak interactions between these adatoms and silicene, therefore, the adsorption energy decrease from V and reaches minimal value at Cr.

As can be seen from Fig. 5, when Sc, Ti, Cr adsorbing on the H site, the density of states (DOS) show peaks at the Fermi level, suggesting a possible Jahn-Teller distortion. In the case of Sc-silicene, we artificially move one of three Si atoms nearest to Sc to break the C_3 rotational symmetry. After relaxation the 3 nearest Si atoms to Sc which originally coplanarly arranged themselves as a regular triangle (d_{Si-Sc} equal to 2.62 Å.) now distort to a isosceles triangle (d_{Si-Sc} become 2.63 Å, 2.63 Å and 3.12 Å.) by pushing the moved Si atom down away from the upper sublattice plane by 1.24 Å. The distorted Sc-silicene system becomes more stable than C_{3v} symmetric one by lowering the total energy by 0.1 eV. Similar to Sc-silicene case, we could expect Jahn-teller distortion to further stabilise Ti-silicene and Cr-silicene systems, never-

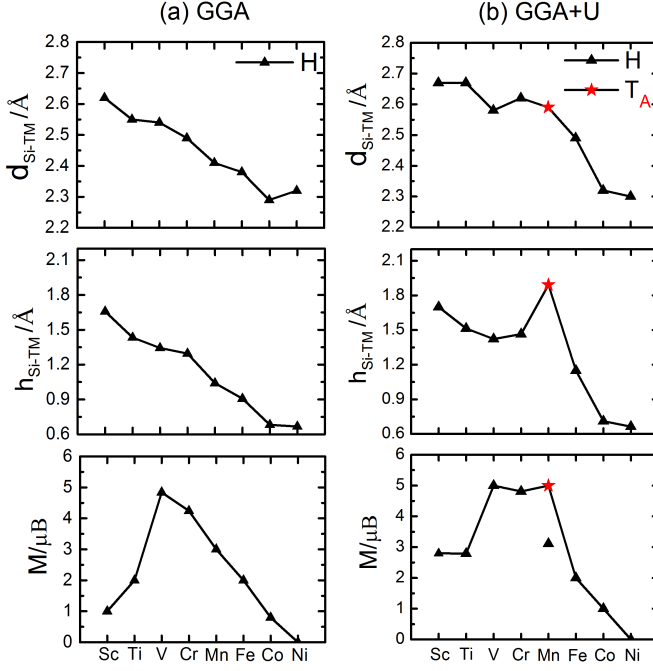


FIG. 3. Structural and magnetic properties of 3d transition metals adsorbed on the Hollow site of 4×4 silicene based on (a) GGA and (b) GGA+ U . For Mn in GGA+ U case, the bond parameters are corresponding to the stablest T_A adsorption site (marked in red pentacle), and the magnetic moment of Hollow and T_A sites are given for comparison.

theless, the distortion for these two system turned out to be rather weak (The modification of position of all atoms is less than 0.005 \AA , and total energy of distorted system which no longer respect the C_{3v} symmetry is lower by $\sim 3 \text{ meV}$).

The resulting magnetic moments and magnetic instability aforementioned can be attributed to the interplay among crystal field splitting, the spin splitting, as well as the electron occupation number of isolated 3d adatoms. For Sc-silicene, the spin splitting for Sc is relatively weak (around 0.2 eV), which is smaller than ligand field splitting between E_2 and A_1 , and totally there are 3 electrons occupying 3d orbitals (see Fig. 5). Therefore, two of these 3 electrons occupy the majority E_2 orbitals and the other one occupies doubly degenerate minority E_2 orbitals, leading to $1 \mu_B$ magnetic moment and potential Jahn-Teller distortion discussed above. For Ti-silicene, owing to the relatively large splitting of A_1 (1 eV), the majority A_1 orbital is occupied before the doubly degenerate minority E_2 orbitals as indicated in inset of Ti's projected density of states (PDOS) from GGA (Fig. 5), resulting in peaks at Fermi level and magnetic moment of $2 \mu_B$. For V, the spin splitting is much larger and high spin state with $5 \mu_B$ moment state is realized, which is essential to the realization of QAHE in silicene as has been discussed before. The other cases can be understood in similar arguments.

When turning on the strong correlation effect, the equilib-

rium structure of adatom-silicene systems are strongly altered compared with GGA case. As can be seen from Fig. 3(b), the $d_{\text{Si-TM}}$, $h_{\text{Si-TM}}$ and $\delta_{\text{Si-TM}}$ for all adsorbates (except Ni) are increased, especially for Ti, Cr, Mn, Fe (the bond lengths for these atoms increased by $\sim 0.1 \text{ \AA}$ while for others by $\sim 0.05 \text{ \AA}$, and the adsorption height also showed noticeable rise for these atoms). And the H site is still favored by most 3d TM (except Mn, which energetically favors T_A site).

The change of adsorption geometry of adatom-silicene system can be attributed to the direct consequence of on-site Coulomb interactions among 3d electrons. In the case of Sc-silicene, the GGA + U predicts $\sim 3 \mu_B$ magnetic moment compared with $\sim 1 \mu_B$ in GGA case (Fig. 3). And the reason for this is the enhanced spin splitting, which results from the effective U , makes spin-up A_1 and E_2 states of Sc occupied as indicated in PDOS of Sc in Fig. 6. For Ti-silicene system, the net magnetic moment is $\sim 3 \mu_B$ rather than $\sim 4 \mu_B$ as one may expected, indicating the $4s$ shell of Ti is empty and about one electron is transferred from Ti to silicene. This is justified by the lowering of Dirac cone at K and $-K$, though slightly distorted, beneath the Fermi level, and occupied PDOS of Si atoms closest to Ti. Similar to Ti-silicene, the Cr-silicene system retained $\sim 5 \mu_B$ magnetic moment after transferring $\sim 1e$ to silicene, which shifts the Dirac cone down by $\sim 0.4 \text{ eV}$ relative to Fermi level. In the case of Mn-silicene, especially, the T_A site is favored if the strong correlation effect is turned on, which is 0.07 eV (0.13 eV) lower in total energy than H (T_A) sites. For V, Fe, Co, Ni, $+U$ mainly enhances the spin splitting while leaving the electron distribution nearly unaffected compared with GGA case, hence the same magnetic moments (Fig. 3).

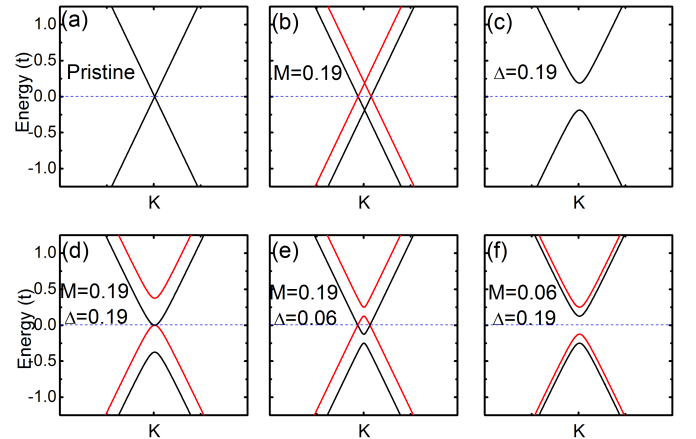


FIG. 4. The evolution of band structure around valley K from the interplay between exchange field M and staggered potential Δ (in unit of t). The red (black) lines are for the majority (minority) spin.

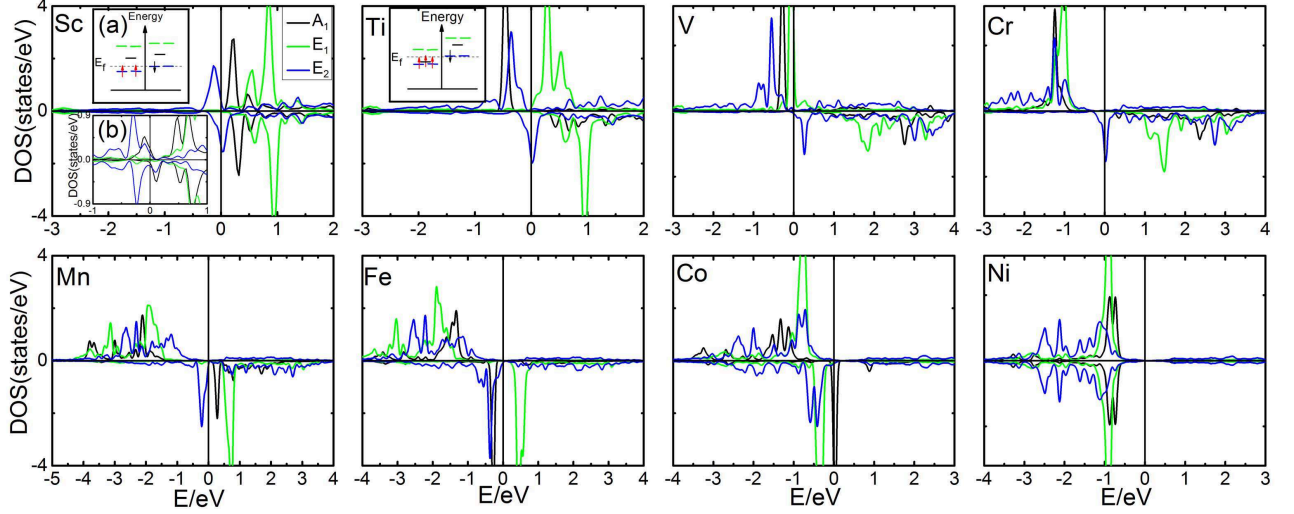


FIG. 5. PDOS of all 3d transition metals adsorbed on the stable site (Hollow) of monolayer silicene from GGA, where positive (negative) values are for majority (minority) spin. The inset (b) in Sc indicates the Jahn-Teller distorted PDOS. The Fermi energy is set to 0 eV.

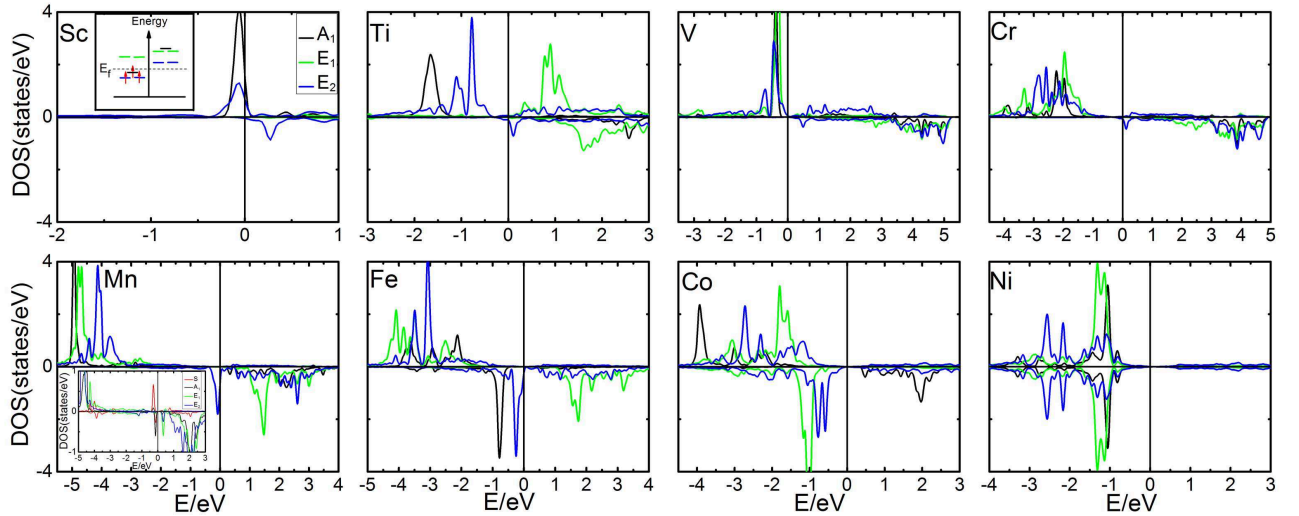


FIG. 6. PDOS of all 3d transition metals adsorbed on the Hollow (H) site of monolayer silicene from GGA+ U (with an effective U being 3.1eV), where positive (negative) values are for majority (minority) spin. For Mn, the PDOS including 4s orbitals are given in inset when absorbing on the stable site T_A . The Fermi energy is set to 0 eV.

BAND STRUCTURE EVOLUTION FROM TIGHT BINDING MODEL

Fig. 4 illustrates the evolution of the band structure around valley K with different combination of exchange field M and staggered potential Δ . Panel(a) shows the band structure of pristine silicene with perfect Dirac-like energy dispersion. In panel(b), the spin degeneracy is lifted when only exchange field M is turned on, rendering crossing of bands with opposite spin around K point in the reciprocal space similar to graphene case [7]. While if only staggered potential Δ is ap-

plied (panel(c)), the system becomes insulating with the valence and conduction bands twofold degenerated.

As mentioned before, in 3d TM doped silicene, the exchange field and staggered potential should appear simultaneously. Panels(d)-(e) indicate the interplay between exchange field (M) and staggered potential (Δ). In the case of panel(d) where $M = \Delta$, there always exists a degenerate point right at the Fermi level. When increasing M and making $M > \Delta$ (panel(e)), the two spin subbands near Fermi level cross, resulting a circular Fermi surface. While if keeps increase exchange field M (panel(f)), the system enters insulating state.

The $M > \Delta$ case is of particular interest in our investigation, since upon turning on the spin orbit coupling effect, the case (e) will give rise to the QAHE and electrically tunable topological states from QAHE to QVHE as discussed before.

-
- [1] P. Hohenberg, and W. Kohn, Phys. Rev. **136**, B864–B871 (1964).
 [2] P. E. Blöchl, Phys. Rev. B **50**, 17953 (1994).

- [3] G. Kresse and J. Furthmüller, Phys. Rev. B **54**, 11169 (1996).
 [4] I. V. Solovyev, P. H. Dederichs, and V. I. Anisimov, Phys. Rev. B **50**, 16861 (1994); V. I. Anisimov, F. Aryasetiawan, and A. I. Lichtenstein, J. Phys. Condens. Matter **9**, 767 (1997).
 [5] S. Cahangirov, M. Topsakal, E. Aktürk, H. Sahin, and S. Ciraci, Phys. Rev. Lett. **102**, 236804 (2009).
 [6] C. C. Liu, W. Feng, and Y. Yao, Phys. Rev. Lett. **107**, 076802 (2011).
 [7] Z. Qiao, S. A. Yang, W. Feng, W. K. Tse, J. Ding, Y. Yao, J. Wang, and Q. Niu, Phys. Rev. B **82**, 161414(R) (2010).

Quantum anomalous Hall effect and tunable topological states in 3d transition metals doped silicene

Xiao-Long Zhang, Lan-Feng Liu, and Wu-Ming Liu

Beijing National Laboratory for Condensed Matter Physics,
Institute of Physics, Chinese Academy of Sciences, Beijing 100190, China

(Dated: October 31, 2018)

We engineer quantum anomalous Hall effect in silicene via doping 3d transition metals. We show that there exists a stable quantum anomalous Hall effect in Vanadium doped silicene using both analytical model and Wannier interpolation. We also predict the quantum valley Hall effect and electrically tunable topological states could be realized in certain transition metal doped silicene where the energy band inversion occurs. Our finding provides new scheme for the realization of quantum anomalous Hall effect and platform for electrically controllable topological states.

PACS numbers: 73.22.-f, 73.43.-f, 75.70.Tj

Introduction.—The recently discovered topological insulators (TIs) [1–5] have aroused great interest in the fields of condensed matter physics and materials science due to the metallic boundary states protected by time-reversal symmetry (TRS). TIs have also become perfect breeding ground for a variety of exotic quantum phenomena [1, 2]. In particular, breaking the TRS respected by TIs via magnetic doping is predicted to give birth to the Majorana fermion [6], topological magnetoelectric effect [7], and the so-called quantum anomalous Hall effect (QAHE) [8–12], which has quantised Hall conductance in the absence of external field [13] and can be intuitively thought as half of TIs. Since TIs have been fabricated in materials ranging from 2D [14] to 3D [15], engineering these novel phenomena in real materials represents one of the most fascinating areas in this field.

As the 2D TI (also known as quantum spin Hall (QSH) insulator) graphene [3, 4, 16] has been altering the research direction of nanoelectronics from silicon-based materials to carbon-based ones, however, the advent of silicene [17–21], which is the silicon equivalent for graphene, seems to turn the tide. Silicene is closely analogous to graphene in the sense that it consists of a single layer of Si atoms arranged to a low buckled honeycomb lattice, and its low energy physics can be described by Dirac-type energy-momentum dispersion akin to that in graphene [17], hence the inherited many intriguing properties, including the expected Dirac fermions and QSH effect [22]. Yet a striking difference between silicene and graphene is that the stable silicene monolayer has additional buckling degree [17], which accounts for the relatively large (1.55 meV) spin orbit coupling (SOC) induced gap [22] in silicene and a couple of unusual quantum phenomena recently reported [23–25]. Indeed, these features together with the natural compatibility with current silicon-based microelectronics industry make silicene a promising candidate for future nanoelectronics application. Moreover, from the view of practical applications, it is highly appreciated if magnetism or sizable band gap or both, like in QAHE with additional edge states protected by topology, can be established in the nonmagnetic silicene, especially in the presence of the buckling degree.

In this Letter, we present a systematic investigation of the adsorption properties and magnetism of 3d transition

metals (TM) doped silicene. We demonstrate that 3d TM strongly bonding with silicene and the TM-silicene systems are strongly magnetic. From combined tight-binding (TB) model analysis and first-principles Wannier interpolation, we investigate the topological properties of the resulting TM-silicene systems. Our results suggest the V doped silicene hosts a stable QAHE, and this system can also be half-metallic [26] if the Fermi level is properly tuned. Further, a close study of the TB model in the band inverted regime gives rise to another topologically nontrivial state, which supports quantum valley Hall effect (QVHE) [27]. We predict the resulting QAHE and QVHE can be tuned directly using an external electrical field.

Adsorption and magnetism analysis.— We use 4×4 supercell of silicene to model the interaction between 3d TM (Sc, Ti, V, Cr, Mn, Fe, Co, Ni) and silicene. As silicene has buckled geometry, we consider three high symmetry adsorption sites, namely the hollow (H) site at the center of a hexagon, two top sites denoted as T_A and T_B corresponding to the top of Si atoms belonging to A and B sublattice, respectively (see Fig. 1). To evaluate the effect of on-site Coulomb interactions among 3d electrons of adatoms on the equilibrium structure and magnetic properties of the TM-silicene system, the simulations have been carried out within generalized gradient approximation (GGA) [31] and GGA+ U [32] framework separately.

Let us first focus on the GGA case. From our first-principles results, of the three adsorption sites concerned, all 3d TM energetically favor H site, which is 0.02 eV \sim 0.60 eV and 0.20 eV \sim 0.80 eV higher in adsorption energy (ΔE) [28] than T_A and T_B site, respectively (see Fig. 2 in Ref. [29]). The bondings between 3d TM and silicene are strongly covalent as manifested by a much larger ΔE ranging from 2.44 eV to 4.75 eV. The unusual large ΔE compared with that in graphene case [11, 33] could be related to the covalently more active sp^3 -like orbitals of silicene, which result from the unique buckled geometry.

Much like the graphene case [11, 33], most of TM (except Ni) doped silicene exhibit magnetism with sizable magnetic moments ranging from $\sim 1 \mu_B$ to $\sim 5 \mu_B$. A relatively large magnetic moment is key to the realization of QAHE in silicene

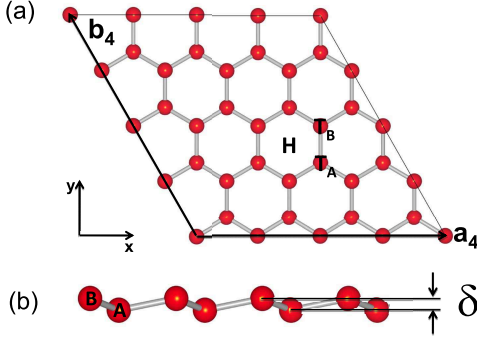


FIG. 1. The lattice geometry of 3d transition metals doped silicene with lattice constant $|a_4| = |b_4| = 4a$, where $a = 3.86 \text{ \AA}$ is the lattice constant of silicene. (a) Top view of 4×4 silicene monolayer where the 3 adsorption sites (Hollow (H), top of A sublattice (T_A) and B sublattice (T_B)) are marked out with black letters. (b) Side view of silicene, the two equivalent Si sublattices are labeled as A and B, respectively, with a buckled distance $\delta = 0.44 \text{ \AA}$.

which we will discuss later. We also note that when some TM (Sc, Ti, Cr) adsorbing on H site, the density of states (DOS) show peaks at the Fermi level, indicating that these systems could be magnetic instable and may undergo Jahn-Teller distortion to lower total energy (especially for Sc, see Ref. [29] for detailed discussion).

The resulting magnetic moments and possible Jahn-Teller distortion aforementioned can be understood in the light of symmetry considerations. When TM are deposited on high symmetry sites of silicene (H, T_A , T_B), the 3d subshell of adatom split into three groups under the C_{3v} symmetric crystal field of system: the $3d_{3z^2-r^2}$ state corresponding to A_1 symmetry group, the twofold degenerate E_1 group consisting of the $3d_{xz}$ and $3d_{yz}$ states and the E_2 group consisting of the $3d_{xy}$ and $3d_{x^2-y^2}$ states. Therefore, the three groups of 3d states hybridise with π orbitals of silicene weakly or strongly according to the different symmetrical properties in similar way as in Benzene [34] and graphene cases [35]. Since 3d orbitals are anti-bonding states, the energy order of them are usually $\epsilon(E_2) < \epsilon(A_1) < \epsilon(E_1)$ and in general $\epsilon(E_2)$ and $\epsilon(A_1)$ are close to each other due to similar hybridization strength with π orbitals. After incorporating spin polarization, the 3 groups of states split, according to different splitting energy, into 10 spin polarized orbitals. Meanwhile, the outer 4s electrons of adatoms experience relatively large electrostatic interaction from the π manifold of silicene than 3d shells due to its spherical symmetry and delocalized nature, making possible charge transfer from the 4s to 3d shells. Thus, the crystal field splitting, spin splitting, together with the occupation number, mostly dominate the electronic structure of adsorbed TM ions (see Ref. [29] for detailed discussion).

Since the strong correlation effect of 3d electrons is not negligible for a practical description of adsorption, we next consider GGA+ U case. After full relaxation, the adsorption geometry of adatom-silicene system is strongly altered com-

pared with GGA case (see Fig. 3(b) in Ref. [29]). And most 3d TM still favor H site (except Mn, which now energetically favors T_A site). Clearly, the geometry change of adatom-silicene systems are the direct consequence of on-site Coulomb interactions among 3d electrons, which modify the electron distribution in 3d and 4s shells of adatoms and π orbitals of silicene as can be seen from the changes of magnetic moments (see Ref. [29] for detailed discussion).

Effective model and Chern number analysis.—In this part, we turn to the main finding of this work, namely the QAHE in the absence of external field via doping 3d TM and the prediction of electrically tunable topological states. As has been shown in Refs. [11, 12], the QAHE could be realized via doping certain 3d or 5d adatoms on the hollow site of graphene. In Fe doped graphene case [11], the QAHE gaps occurs around the Dirac K points of the Brillouin zone, and the low energy physics can be described by a Hamiltonian for graphene in the presence of extrinsic Rashba SOC (λ_R^{ext}) and exchange field (M) [36] introduced solely by the adatom. Here in silicene, however, owing to the low buckled structure, there exists intrinsic Rashba SOC (λ_R^{int}) [30]. Moreover, when depositing 3d TM on the stable adsorption site, the induced inequality of AB sublattice potential (Δ) necessarily arise and compete with magnetization. Below we identify conditions for the realization of QAHE in silicene based on a effective Hamiltonian [30] by introducing a staggered AB sublattice potential besides SOC (λ_R^{ext} and λ_{so}) and exchange field (M). In the basis of $\{|A, B\rangle \otimes \{|\uparrow, \downarrow\rangle\}$, the Hamiltonian reads:

$$H_{eff}^{\pm} = H_s^{\pm} + H_d^{\pm}, \quad (1)$$

with $H_s^{\pm} = \epsilon_{eff}\tau_0 \otimes \sigma_0 \pm \tau_3 \otimes h_{11} + \hbar v_F(k_x\tau_1 \mp k_y\tau_2) \otimes \sigma_0$, $H_d^{\pm} = \lambda_R^{ext}(\pm\tau_1 \otimes \sigma_2 - \tau_2 \otimes \sigma_1) + \Delta\tau_3 \otimes \sigma_0 + M\tau_0 \otimes \sigma_3$, $h_{11} = -\lambda_{so}\sigma_3 - a\lambda_R^{int}(k_y\sigma_1 - k_x\sigma_2)$, where H_{eff}^{\pm} are the total Hamiltonian for the two inequivalent Dirac points $K(+)$ and $-K(-)$, H_s^{\pm} are the low energy effective Hamiltonian for the QSH insulator silicene, H_d^{\pm} include all the effects introduced by the 3d dopants, including effective spin-dependent magnetic field M , site-dependent staggered potential Δ and the resulting extrinsic Rashba SOC λ_R^{ext} . The τ and σ are the Pauli matrices acting separately on pseudospin (sublattice) and spin space, ϵ_{eff} stands for the $\epsilon_1 - \lambda_{2nd}$ term in Ref. [22], v_F and a are the Fermi velocity and the lattice constant, respectively, and λ_{so} is the effective SOC.

By diagonalizing the above Hamiltonian, the electronic structure around each valley (K and $-K$) in Brillouin zone can be obtained (the ϵ_{eff} term can be safely ignored). From the interplay between exchange field (M) and staggered potential (Δ) (see Fig. 4 in Ref. [29]), we conclude that energy bands with opposite spin intersect, which is essential to the QAHE in Fe doped graphene, only when $M/\Delta > 1$. This is different from that in Ref. [36], where $\Delta = 0$ and there always exists 2 degenerate points around Dirac point as long as $M \neq 0$.

We found that either the extrinsic or the intrinsic Rashba SOC would lead to insulating state when starting from the case $M/\Delta > 1$. To identify the topological properties of the resulting insulating state, we resort to the Chern number (C)

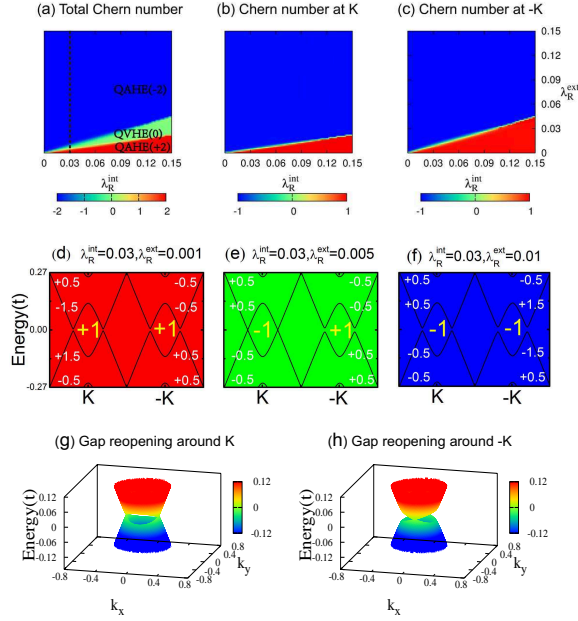


FIG. 2. The transition of Chern number by tuning λ_R^{ext} and λ_R^{int} (in unit of t). (a) Three topological nontrivial states, QAHE(2), QVHE(0) and QAHE(-2) with Chern number +2, 0, and -2, can be obtained from different combination of λ_R^{ext} and λ_R^{int} . (b) and (c) represent the variation of C_K and C_{-K} . (d), (e) and (f) depict the band structure along $k_y = 0$ line in BZ for the three topological states (QHE(2), QVHE(0) and QHE(-2)) in (a). The yellow integers (± 1) represent C_K and C_{-K} , corresponding to the sum of topological charge of each valence bands (the white ± 0.5 and ± 1.5). (g) and (h) show the gap closing around K and $-K$. They are the transition states from QAHE(+2) to QVHE(0) and from QVHE(0) to QAHE(-2), respectively.

analysis [37]. The C can be obtained by the integral over the first Brillouin zone (BZ): $C = \frac{1}{2\pi} \int_{BZ} \Omega(\mathbf{k}) d^2k$. The $\Omega(\mathbf{k})$ is the usual Berry curvature of all occupied states [38]:

$$\Omega_z(\mathbf{k}) = -2 \sum_n \sum_{m \neq n} f_n \text{Im} \frac{\langle \psi_{n\mathbf{k}} | v_x | \psi_{m\mathbf{k}} \rangle \langle \psi_{m\mathbf{k}} | v_y | \psi_{n\mathbf{k}} \rangle}{(\epsilon_{m\mathbf{k}} - \epsilon_{n\mathbf{k}})^2}, \quad (2)$$

where f_n is the Fermi-Dirac distribution function for band n , $\psi_{n\mathbf{k}}$ is the Bloch function of eigenenergy $\epsilon_{n\mathbf{k}}$, v_x , v_y are the velocity operators. And anomalous Hall conductivity is readily given by $\sigma_{xy} = (e^2/h)C$. Interestingly, the extrinsic Rashba SOC (λ_R^{ext}) gives insulating state with $C = +2$ while the intrinsic one (λ_R^{int}) leads to that with $C = -2$. One may expect that different Chern number state can be realized if tuning the two types of Rashba SOC properly in experiments. Fig. 2(a) indicates that this is indeed the case, where C can take integer value of +2, 0, -2 with different combination of λ_R^{int} and λ_R^{ext} . Careful study shows that the tunable C originates from different response of bulk gap to the 2 types of Rashba SOC (λ_R^{int} and λ_R^{ext}) around K and $-K$. When increasing λ_R^{ext} while keeping λ_R^{int} fixed, for example, at $0.03t$ ($t = 1.6$ eV is the nearest neighbor hopping parameter [30]) as shown in Fig. 2(a), we can see clearly the transition of Chern number of each valley

(C_K and C_{-K}) from +1 to -1 but with different rate, i.e., C_K experiences a topological transition earlier than C_{-K} (see Figs. 2(b)-2(c)). The step change of C_K and C_{-K} is justified by the observation of bands touching and gap reopening around each valley (Figs. 2(d)-2(f)). Notice that the rotational symmetry of the effective Hamiltonians along z direction in any angle is broken after bringing in the Rashba SOC terms, and hence the band touching happens only on $k_y = 0$ line in BZ for valley K (Fig. 2(g)) while $k_x = 0$ line for valley $-K$ (Fig. 2(h)). Consequently, the system can be in QAHE phase (with C being +2 or -2) or QVHE (with C being 0 and $C_K = -C_{-K} = -1$) depending on different value of λ_R^{ext} , which is controllable through an external gate voltage.

The effective SOC (λ_{so}), however, further breaks the particle-hole symmetry of the above Hamiltonian, making energy bands shift up (at valley K) or down (at valley $-K$) relative to the Fermi level while leaving the topological charge of each valley unchanged. Hence, as long as the shifting is small, the system is still insulating and the above discussion of topological transition remain valid.

Some of the topologically non-trivial phases can be realized in 3d TM doped silicene as predicted by our first-principles calculations. For example, we notice that the opposite spin subbands cross around the Fermi level in V, Cr, Mn doped silicene due to relatively large magnetization. Meanwhile, for these systems the spin-up and spin-down subbands near Fermi level are also gapped (Fig. 3(a1) and Fig. 3(a3)), which makes these systems candidates for half-metallic materials if tuning Fermi level properly. We take V-silicene as a prototype and discuss in detail, as this system is insulating with an energy gap around 6meV (Fig. 3(a2)) when only the SOC is turned on. We find the SOC induced band gap in V-silicene is stable even strong correlation effect of V is considered by including effective U value ranging from 0 to 6 eV (Fig. 3(a4)).

To obtain an accurate Berry curvature distribution and hence Chern number in first-principles level in V doped silicene, the Wannier interpolation technique have been used [39, 40]. The band structure from first principle is well reproduced by interpolation as indicated in Fig. 3(a4). In Fig. 3(b), the Berry curvature ($\Omega_z(k)$) in k -space is explicitly shown. As we may observe, the most nonzero values of Berry curvature distribute around the Dirac K points by forming small circles, where exactly the avoided crossing happens (Fig. 3(a4)). By the integral over BZ, we indeed find the Chern number of all occupied bands equals to an integer value of +2, which signals the V doped silicene is in QAHE phase.

For the proposed QVHE state in former model analysis, we note that the λ_R^{int} is rather small (being about $4.4 \times 10^{-4}t$) [30]. Therefore, the QVHE region in Fig. 2(a) would be quite small and it may not be easy to directly observe the QVHE from experiment. To tide it over, putting V-silicene system or its counterpart of TM doped Germanium on substrate may be a feasible solution.

Conclusions.—To summarize, we have demonstrated that the 3d TM doped silicene can be intriguing materials as manifested by the induced strong magnetic moments, potential

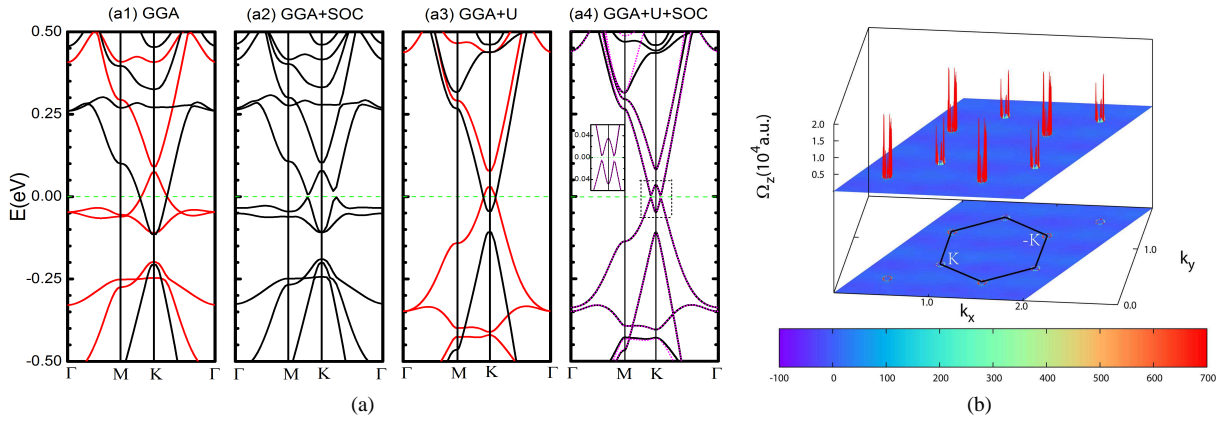


FIG. 3. (a) The band structures of V doped silicene from GGA ((a1)-(a2)) and GGA+ U ((a3)-(a4)), respectively. The red (black) color in (a1) and (a3) correspond to majority spin (minority spin) subbands. After including SOC effect, a gap is opened at the Fermi level ((a2) and (a4)). In (a4), the band structure from Wannier interpolation is also shown in pink dashed lines. (b) The distribution of Berry curvature ($\Omega_z(k)$) in V doped silicene from GGA+ U +SOC. The BZ is marked out with black hexagon.

half-metallic property as well as sizable topologically non-trivial gaps. These features have also been confirmed in the presence of strong correlation effect of 3d TM. Moreover, we predicted the emerging of electrically controllable topological states (QAHE and QVHE phases as characterized by different Chern number) in certain TM-silicene systems where the energy bands are being inverted. Our work may provide new candidate for the long-sought QAHE and platforms to manipulate topological phase transition electrically.

X. L. Zhang acknowledges very helpful discussions with H. M. Weng, Y. G. Yao, C. C. Liu and J. J. Zhou. This work was supported by the NKBRSCF under grants Nos. 2011CB921502, 2012CB821305, 2009CB930701, 2010CB922904, NSFC under grants Nos. 10934010, 11228409, 61227902 and NSFC-RGC under grants Nos. 11061160490 and 1386-N-HKU748/10.

[1] X. L. Qi, and S. C. Zhang, Rev. Mod. Phys. **83**, 1057 (2011).
[2] M. Z. Hasan, and C. L. Kane, Rev. Mod. Phys. **82**, 3045 (2010).
[3] C. L. Kane, and E. J. Mele, Phys. Rev. Lett. **95**, 226801 (2005).
[4] C. L. Kane, and E. J. Mele, Phys. Rev. Lett. **95**, 146802 (2005).
[5] B. A. Bernevig, T. A. Hughes, and S. C. Zhang, Science **314**, 1757 (2006).
[6] L. Fu, and C. L. Kane, Phys. Rev. Lett. **102**, 216403 (2009).
[7] X. L. Qi, T. L. Hughes, and S. C. Zhang, Phys. Rev. B **78**, 195424 (2008).
[8] X. L. Qi, Y. S. Wu, and S. C. Zhang, Phys. Rev. B **74**, 085308 (2006).
[9] C. X. Liu, X. L. Qi, X. Dai, Z. Fang, and S. C. Zhang, Phys. Rev. Lett. **101**, 146802 (2008).
[10] R. Yu, W. Zhang, H. J. Zhang, S. C. Zhang, X. Dai, and Z. Fang, Science **329**, 61 (2010).
[11] J. Ding, Z. Qiao, W. Feng, Y. Yao, and Q. Niu, Phys. Rev. B **84**, 195444 (2011).
[12] H. Zhang, C. Lazo, S. Blügel, S. Heinze, and Y. Mokrousov, Phys. Rev. Lett. **108**, 056802 (2012).

[13] F. D. M. Haldane, Phys. Rev. Lett. **61**, 2015 (1988).
[14] M. König, S. Wiedmann, C. Brune, A. Roth, H. Buhmann, L. W. Molenkamp, X. L. Qi and S. C. Zhang, Science **318**, 766 (2007).
[15] H. J. Zhang, C. X. Liu, X. L. Qi, X. Dai, Z. Fang, and S. C. Zhang, Nature Phys. **5**, 438 (2009).
[16] K. S. Novoselov, A. K. Geim, S. V. Morozov, D. Jiang, M. I. Katsnelson, I. V. Grigorieva, S. V. Dubonos, and A. A. Firsov, Nature **438**, 197 (2005).
[17] S. Cahangirov, M. Topsakal, E. Aktürk, H. Sahin, and S. Ciraci, Phys. Rev. Lett. **102**, 236804 (2009).
[18] B. Aufray, A. Kara, S. Vizzini, H. Oughaddou, C. Leandri, B. Ealet, and G. L. Lay, Appl. Phys. Lett. **96**, 183102 (2010).
[19] B. Lalmi, H. Oughaddou, H. Enriquez, A. Kara, S. Vizzini, B. Ealet, and B. Aufray, Appl. Phys. Lett. **97**, 223109 (2010).
[20] P. Vogt, P. D. Padova, C. Quaresima, J. Avila, E. Frantzeskakis, M. C. Asensio, B. Ealet, and G. L. Lay, Phys. Rev. Lett. **108**, 155501 (2012).
[21] L. Chen, C. C. Liu, B. J. Feng, X. Y. He, P. Cheng, Z. J. Ding, S. Meng, Y. G. Yao, and K. H. Wu, Phys. Rev. Lett. **109**, 056804 (2012).
[22] C. C. Liu, W. Feng, and Y. Yao, Phys. Rev. Lett. **107**, 076802 (2011).
[23] M. Ezawa, Phys. Rev. Lett. **109**, 055502 (2012).
[24] M. Tahir and U. Schwingenschlögl, Scientific Reports **3**, 1075 (2013).
[25] L. Chen, B. J. Feng, and K. H. Wu, arXiv:1301.1431
[26] M. I. Katsnelson, V. Y. Irkhin, L. Chioncel, A. I. Lichtenstein, and R. A. de Groot, Rev. Mod. Phys. **80**, 315 (2008).
[27] D. Xiao, W. Yao, and Q. Niu, Phys. Rev. Lett. **99**, 236809 (2007).
[28] $\Delta E = E_s + E_{ads} - E_{s-ads}$ is the adsorption energy within GGA, where E_s , E_{ads} , E_{s-ads} are energies of the 4×4 pristine silicene, single adatom, and silicene-adatom system, respectively.
[29] Supplemental materials
[30] C. C. Liu, H. Jiang, and Y. Yao, Phys. Rev. B **84**, 195430 (2011).
[31] P. E. Blöchl, Phys. Rev. B **50**, 17953 (1994).
[32] I. V. Solov'yev, P. H. Dederichs, and V. I. Anisimov, Phys. Rev. B **50**, 16861 (1994); V. I. Anisimov, F. Aryasetiawan, and A. I. Lichtenstein, J. Phys. Condens. Matter **9**, 767 (1997).
[33] K. T. Chan, J. B. Neaton, and M. L. Cohen, Phys. Rev. B **77**,

- 235430 (2008).
- [34] H. M. Weng, T. Ozaki, K. Terakuta, J. Phys. Soc. Jpn. **77**, 014301 (2008).
 - [35] T. O. Wehling, A. V. Balatsky, M. I. Katsnelson, A. I. Lichtenstein, and A. Rosch, Phys. Rev. B **81**, 115427 (2010).
 - [36] Z. Qiao, S. A. Yang, W. Feng, W. K. Tse, J. Ding, Y. Yao, J. Wang, and Q. Niu, Phys. Rev. B **82**, 161414(R) (2010).
 - [37] D. J. Thouless, M. Kohmoto, M. P. Nightingale and M. den Nijs, Phys. Rev. Lett. **49**, 405 (1982).
 - [38] D. Xiao, M. C. Chang, and Q. Niu, Rev. Mod. Phys. **82**, 1959 (2010).
 - [39] A. Mostofi, J. R. Yates, Y.-S. Lee, I. Souza, D. Vanderbilt, and N. Marzari, Comput. Phys. Commun. **178**, 685 (2008).
 - [40] X. Wang, J. R. Yates, I. Souza, and D. Vanderbilt, Phys. Rev. B **74**, 195118 (2006).